Modelling of Disaster Spreading Dynamics

Igor Stanković, Milan Žeželj, Jelena Smiljanić, and Aleksandar Belić

Scientific Computing Laboratory, Institute of Physics Belgrade,
University of Belgrade, Pregrevica 118, 11080 Belgrade, Serbia
igor.stankovic@ipb.ac.rs

Abstract. Natural hazards are significant problem that every year cause important loses. We report on both theoretical models and simulations aimed at better understanding of disaster spreading in various networks. The structure of the networks in this work is obtained either through neighbor analysis in real space or using models which reproduce generic features of real networks (i.e., power, telecommunication, or road networks). Our investigations are focused on the understanding of interaction between network structure and disaster spreading mechanism. The probability that fire will propagate through fire protection strip is investigated and a model is introduced based on finite-size considerations in percolation theory. Also, the uncertainty in prediction of fire propagation rate due to the local inhomogeneities of the vegetation cover is investigated. Finally, uncertainty in cascade failures of network infrastructure is analyzed for a model where edges have limited capacity. The importance of the results for disaster prevention and control is discussed as well.

1 Introduction

The design of prevention measures and distribution of resources needed for efficient response to disaster event is a challenging problem. Examples include control of fire propagation [1], power transmission grid failure [2], information loss in communication systems [3, 4], and traffic congestions [5]. Development of new strategies for infrastructure failure prevention and damage control, such as emergency response and recovery call for external resources, which are limited, is important topic with many practical implications in real systems. A considerable research effort is underway to improve understanding of interaction of the structure and disaster propagation which considerably contributes to the understanding of processes going on in these networks. Experimental studies of disasters under real conditions are performed but understandably at scales much smaller then real disasters [7]. it is not realistic to expect allocation of resources for systematic data gathering during the disasters. Therefore mathematical and computer models are often very helpful tools to extend human knowledge beyond limited input data. However, the complexity of systems struck by disasters does not allow one to model the interactions of all involved entities and processes in detail and especially not in real time. Therefore, we have to capture them by an appropriate generic model. During 80's a line of research was initiated in which

M. Dulea et al. (eds.), *High-Perf. Comp. Infrastr. for South East Europe's Research Communities*, Modeling and Optimization in Science and Technologies 2,
DOI: 10.1007/978-3-319-01520-0_4,

model were used that reproduce and explain vegetation recovery and fire spread distribution in quite abstract way [8, 10]. These lattice models were used to describe fire size distributions which have a power law form [9, 10].

In this proceeding we report on our recent efforts to develop both theoretical models and simulations aimed on better understanding of disaster spreading and control in various networks. The structure of the networks is obtained either through neighbor analysis in real space or using models which reproduce generic features of real networks (i.e., power, telecommunication, or road networks) [3, 11–13]. The percolation and transport models on networks can be used to evaluate the disaster probability and impact. This information is important in practice for deciding how to effectively distribute resources in order to fight disasters the best. For example, finite size scaling considerations in percolation theory can be directly applied to design fire spreading prevention routes. In case of the fire behavior predictions uncertainty comes from variability in weather and fuel (vegetal) state inputs. Commonly model assumptions, such as fuel homogeneity and steady-state spread, limit the capability of the fire propagation models to provide reliable results, possibly leading to uncertainties of unknown magnitude [14]. We introduce a simple off-lattice deterministic reaction-thermal diffusion model in order to describe the dynamical evolution of the fire. Introduced model is not so specific as those employed by the ecologists but still introduces fire activation energy and heat dissipation. The model has an advantage that it can be applied in real time. We demonstrate how this simple model can provide interesting information about dynamics of the forest fire propagation. In the final part of proceeding we present a model of cascading failure. Cascading failure can happen in many infrastructure networks, including the electrical power grid, the Internet, road systems, and so on. The phenomenon is refereed to us an avalanching type of process, where the failure of a single or of a few network components can result in a large-scale breakdown of the network. In recent years cascading breakdown in complex networks has received considerable attention [2, 15–21]. Most previous existing works on cascading failures only focused on attacks on nodes rather than on edges. Attacks on edges are as important for the network security as those on nodes, and therefore deserve a careful investigation. In this proceeding, we analyze the cascade of overload failures in complex networks, where a edge failure and a subsequent network-wide redistribution of loads might trigger further cascading failures.

The proceeding is organized as follows: in Sec.2 we investigate the fire percolation probability dependence on density and shape of fire control paths. Based on finite size considerations in percolation theory we derive a simple model for assessment of fire propagation risk through corridor. In Sec.3, deterministic reaction-thermal diffusion model is introduced and simulation results for different vegetal phase densities are presented. Cascade of overload failures in complex networks are analyzed in Sec.4. Conclusion is given in Sec.5.

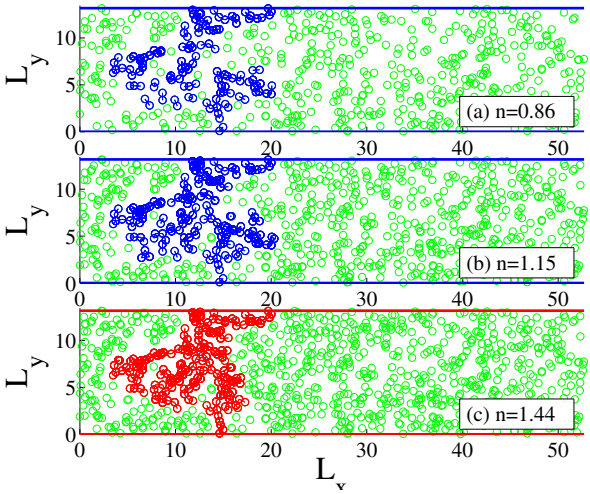

Fig. 1. The snapshots of evolution of two dimensional (2D) system as new circles representing tree crowns or bush are added and overall number density increases n. Two tree crowns or bush lie in the same cluster if the representing circles intersect. At lower densities (a) $n = 0.86$ and (b) $n = 1.15$ there is no percolating cluster in y direction. Circles that will form percolating cluster are blue while others are green. As density increases percolating cluster (red) is created, cf. (c) $n = 1.44$.

2 Percolation Probability Density

Monte Carlo simulations, coupled with an efficient cluster analysis algorithm and implemented on grid platform, are used to investigate the fire percolation probability dependence on density of a vegetation phase, and the surface geometry (shape) [22–25]. We consider two dimensional (2D) systems with isotropically placed circles representing tree crowns or bushes. Circles have all same unit radius and are randomly positioned and oriented inside the rectangular field of width L_x and height L_y. Two tree crowns or bushes lie in the same cluster if the representing circles intersect. System percolates if two opposite boundaries are connected with the same cluster, see Figure 1. The aspect ratio r is defined as the length of the rectangular system in percolating direction divided with the length in perpendicular direction. We define the normalized system size as a square root of the rectangular area $L = \sqrt{L_x L_y}$ (geometric average), which represent the length of the square system with the same area. The percolation behavior, i.e., the probability that will be able to find path to propagate, is studied in terms of the vegetation density $n = N/L^2$ where N is total number of trees/bushes.

From Fig. 2, one can see that average percolation density $\langle n \rangle_{L,r}$ for aspect ratio higher than one is monotonically decreasing function of the system size L. Somewhat surprising, for aspect ratios lower than one, $\langle n \rangle_{L,r}$ is not monotonic function and has local minimum. For small systems $\langle n \rangle_{L,r}$ is a decreasing function, which passes through n_c, reaches a minimum and after that converges to n_c from below. From general scaling arguments one would expect that for all finite

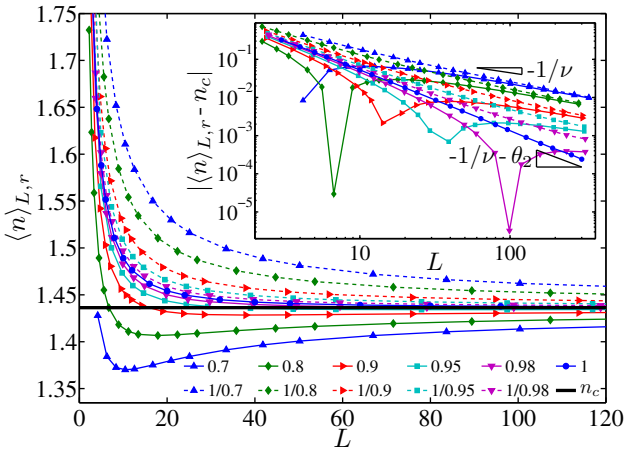

Fig. 2. The average percolation density $\langle n \rangle_{L,r}$ dependence on the system size L and aspect ratio r. The values are obtained from Monte Carlo simulations and calculated using Eq. (1). The values are given for aspect ratios $r = 0.7, 0.8, 0.9, 0.95, 0.98, 1$ (solid lines) and their inverse values $r = 1/0.7, 1/0.8, 1/0.9, 1/0.95, 1/0.98$ (dashed lines). The bold line denotes the expected values for the percolation threshold n_c. Inset: The same data is shown in logarithmic scale to demonstrate the same power law convergence of the r and $1/r$ pairs.

systems their convergence is governed by an exponent $-1/\nu$. For two-dimensional (2D) systems $\nu = 4/3$ [26].

Further it was showed that for lattice percolation on the square system leading exponent of the average concentration at which percolation first occurs is $-1/\nu - \theta$, where $\theta \approx 0.9$ [27]. These studies were performed for symmetric systems. In inset of Fig. 2, one can see that for large system sizes all the curves show power law convergence to percolation threshold n_c with exponent $-1/\nu$, except in the symmetric case, i.e., $r = 1$, where exponent is $-1/\nu - \theta_1$. Absolute values of the leading-order prefactors are the same for aspect ratios r and $1/r$.

The scaling behavior of the $\langle n \rangle_{L,r}$ can be described with generalized moment scaling function with aspect ratio dependent coefficients

$$\langle n \rangle_{L,r} = n_c + L^{-1/\nu} \sum_{i=1}^{\infty} a_i(r) L^{-\theta_i}, \tag{1}$$

where θ_i are generalized corrections to scaling exponents [31]. The coefficients of the first two order terms have form $a_1(r) \approx a_{1,1}\ln(r) + a_{1,2}\ln^3(r)$ and $a_2(r) \approx a_{2,1} + a_{2,2}\ln^2(r)$ (for detailed derivation of expression see Ref. [13]). The previous expansion implies a faster then $L^{-1/\nu}$ convergence of average percolation density $\langle n \rangle_{L,r}$ of symmetric system to its infinite-system value, characterized by an exponents θ_1. The standard deviation $\Delta_{L,r}$ can be described with expansion

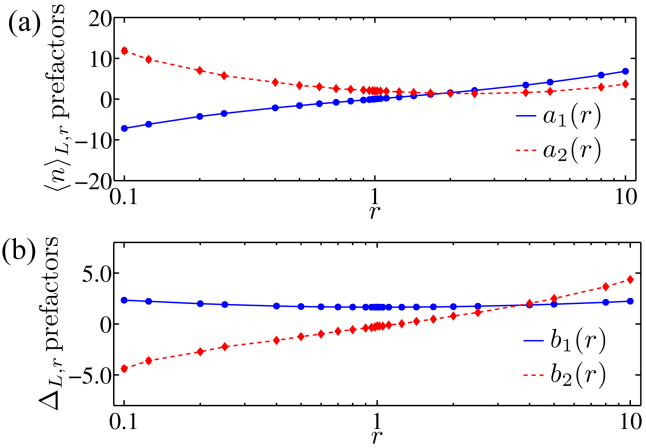

Fig. 3. Prefactors are shown for the two leading-order terms of generalized scaling function for average percolation density $\langle n \rangle_{L,r}$ (upper graph) and standard deviation $\Delta_{L,r}$ (lower graph). The first order prefactor of average percolation density is odd function on logarithmic scale, i.e., $a_1(r) = -a_1(1/r)$ and the first order prefactor of standard deviation is even function, i.e., $b_1(r) = b_1(1/r)$.

$$\Delta_{L,r} = L^{-1/\nu} \sum_{i=1}^{\infty} b_i(r) L^{-\theta_i}. \tag{2}$$

As one would expect, standard deviation is monotonically decreasing function of the system size L. The coefficients of the first two order terms have form $b_1(r) \approx b_{1,1} + b_{1,2}\ln^2(r)$ and $b_2(r) \approx b_{2,1}\ln(r) + b_{2,2}\ln^3(r)$, cf. Ref. [13].

From Monte Carlo simulation data we have obtained the first and second order terms of $\langle n \rangle_{L,r}$ in Eq. (1) by interpolation. Results of the analysis are shown in Fig. 3(a) and coefficients are given in Table 1. The influence of higher order terms were comparable or smaller then simulation data error and we could not extract them with sufficient precision. We obtain that the first order correction θ_1 is equal zero, as predicted by general scaling arguments in Ref. [26]. For the second order correction, we obtain $\theta_2 = 0.83(2)$ for $r = 1$. The residual aspect ratio dependence of θ_2 cannot be further analyzed without provision of retaining the first two terms in Eq. (1). The variance prefactors for two leading terms are shown in Fig. 3(b). The fitting coefficients $b_{i,j}$ are given in Table 1.

To illustrate impact of previous conclusions, we calculate safe (maximal) vegetation density n_{max} in fire protection strips. The results are given in Figure 4 for percolation probability tolerances $p = 15.73\%$ and 0.01%, i.e., probabilities that fire will find a passage. The curves are calculated using average value and standard deviation given in Eq. (1) and (2). Probability density function is approximated with normal distribution. It is helpful to understand that the maximal vegetation density depends on logarithm of strip length. This means that even for $L_x = 100L_y$ there is a high tolerance for vegetation density $n_{max} \approx 0.45$ for which probability of fire finding path through the strip is less then 0.01%.

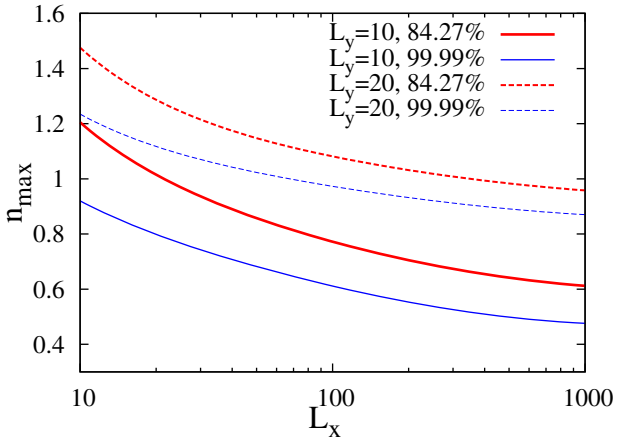

Fig. 4. Safe (maximal) vegetation density n_{max} in fire protection strips for which percolation probability is $p = 15.73\%$ (red) and 0.01% (blue). The curves are calculated using average value and standard deviation given in Eq. (1) and (2).

Table 1. Results for coefficients $a_{i,j}$ and $b_{i,j}$, where $i, j \in 0, 1$. The results are obtained using the least-square method.

	1,1	1,2	2,1	2,2
$a_{i,j}$	2.5(1)	0.11(3)	2.2(7)	1.0(3)
$b_{i,j}$	1.61(3)	0.14(1)	1.35(8)	0.11(2)

3 Fire Spreading on Percolating Networks

In this section we further extend percolation model to include combustion effects, where the whole forest/bush (i.e., vegetation and gases) is described with an equivalent point values at positions of its constituting parts. The assumptions for introducing this simple model are the following: The forest at the macroscopic scale can be considered as a random medium, with density n. This random medium, called vegetal phase, is composed of fuel (e.g., trees, trunks, bushes, etc.). One can consider that one of the main process in forest fire is heat transfer by radiation and convection. We consider that heat transfer is only possible between neighboring trees/bushes, all of the same unit radius. The main effects of the heat transfer are drying of the vegetation and vegetation pyrolysis that produce heat. We assume that hydrodynamics of gas which allows to bring the oxygen necessary to the combustion is fast and homogeneous. The energy released in pyrolysis leads to forest fire propagation.

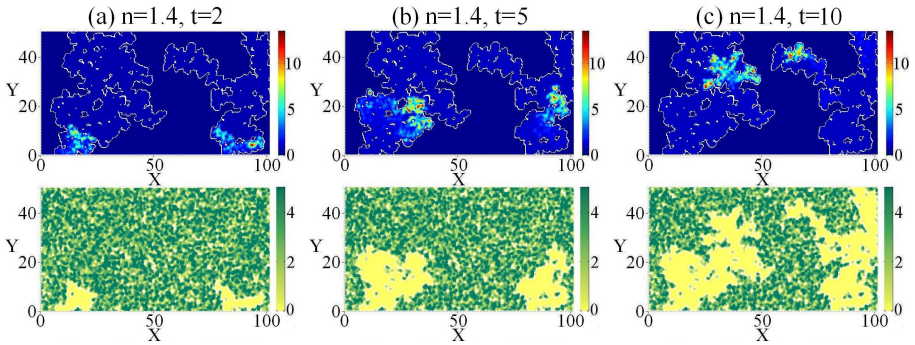

Fig. 5. Snapshots visualizing the propagation of fire through vegetal phase at $t = 2, 5,$ and 10. System has initial vegetal phase density $n = 1.4$ and fire is initiated at its lower boundary. Upper plot represents local temperature distribution and lower local vegetal phase density.

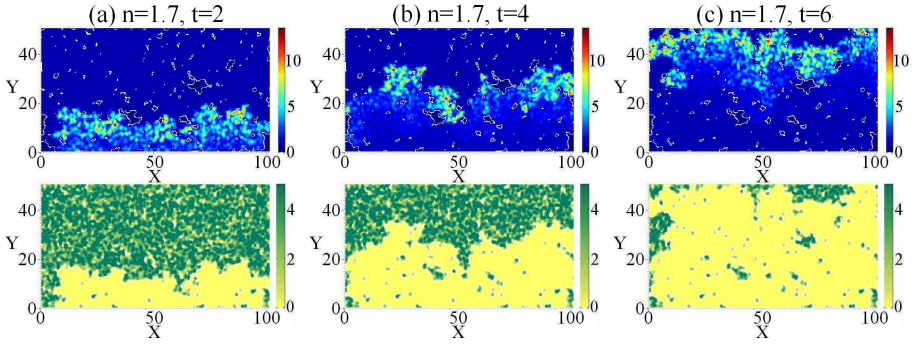

Fig. 6. Snapshots visualizing the propagation of fire through vegetal phase at $t = 2, 4,$ and 6. System has initial vegetal phase density $n = 1.7$ and fire is initiated at its lower boundary. Upper plot represents local temperature distribution and lower local vegetal phase density.

We have simplified the general model introduced elsewhere, cf. Ref. [28–30], in order to obtain the following system of equations. The balance of energy or thermal equation is

$$\frac{\partial T_{\mathrm{f}}^{j}}{\partial t} = \lambda_{\mathrm{f}} \triangle T_{\mathrm{f}}^{j} + R^{j} + \lambda_{\mathrm{i}}(T_{\mathrm{f}}^{j} - T_{\mathrm{i}}), \tag{3}$$

where T_{f} is temperature of vegetal phase at mass point j, λ_{f} equivalent heat conductivity between vegetal phase, λ_{i} equivalent heat conductivity to environment and T_{i} environment temperature. We assume for simplicity parabolic temperature distribution between neighboring points. The pyrolytic heat source is given by $R^{j} = (k(T_{\mathrm{f}}^{j})/C_p)Y_{\mathrm{f}}^{j}$ where Y_{f}^{j} is fraction of vegetation phase in mass point, C_p effective heat capacity and k is reaction rate. In the present model $Y_{\mathrm{f}}^{j} = 1$ is corresponding to the vegetation phase green at the mass point and $Y_{\mathrm{f}}^{j} = 0$ burned. Reaction rate $k(T)$ is defined by the standard Arrhenius expression,

i.e., $k(T) = Be^{-E_A/k_B T}$, where B is prefactor, k_B Boltzmann constant and E_A activation energy. The balance of mass at point j is written generically

$$\frac{\partial Y_f^j}{\partial t} = -k(T_f^j)Y_f^j. \tag{4}$$

Comparison of fire propagation between two simulations is given in Figures 5 and 6. The two simulations have identical inputs $E_A/k_B = 0.1$, $B = 1000$, $\lambda_i = 1.2$, $\lambda_f = 1.$ and $C_p = 10.$ but different spatial densities $n = 1.4$ and 1.7. The fire is initiated at its lower boundary. As one could expect, at lower density $n = 1.4$ not whole surface can be visited by the fire. Still, we observe that in both cases fire propagation is not homogeneous and it depends on local structure of the vegetation phase. We also observe a local auto-extinction events. The fire is spreading faster through the clusters of vegetation phase, and it slows down when vegetation becomes rate. Therefore differences in propagation are not large inside clusters; differences in variance in spread rate is only significant between vegetation clusters. Therefore, at higher densities where connections between vegetation clusters are abundant fire spread rate is less variable, cf. Figure 7.

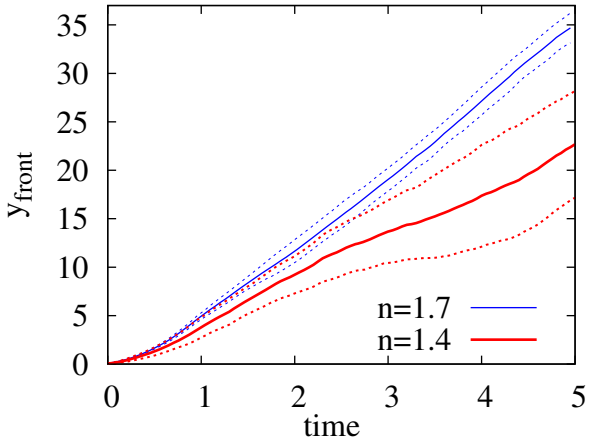

Fig. 7. Evolution of the fire front in time for two vegetation densities $n = 1.4$ and $n = 1.7$. Bold line represents mean value of fire front position y_{front} and dashed lines are delimiting 68% confidence band ($y_{front} \pm \sigma$).

4 Cascade Failures

In the present proceeding we adopt the model of cascading failures caused by overload presented in [2] to investigate the overload breakdown problem when edges (rather than nodes) are sensitive to overloading. Within this model, it is assumed that, at each time step, every node provides (receives) flow to (from) every other node of the network with an equal share and the flow is forwarded

along the shortest path. The edge's initial load L is defined by means of the betweenness centrality, which describes the number of all shortest paths through the edge. The capacity C_i of edge i, which defines the maximum load that the edge can handle at each time step, is set to be proportional to the edge initial load $C_i = (1+\alpha)L_i$, where the constant $\alpha \geq 0$ is a tolerance parameter. An edge is overloaded and fails if $L_i > C_i$. When for any reason an edge fails, the traffic which used to go through this edge is redistributed to a new shortest path. This results in a network-wide redistribution of traffic load. As a consequence of this redistribution, some edges have to carry a larger load than before. If this new load exceeds the capacity of these edges, then the respective edges will also fail, triggering a new load redistribution with possible, subsequent overload failures of other edges. This eventually leads to a cascade of failures, after which only a fraction of the nodes is still functioning. This fraction does not necessarily form a connected network. The largest of these subnetworks, i.e., the one containing the largest number of nodes, is called the giant component G.

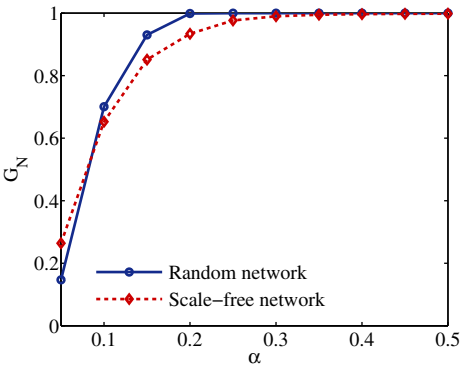

Fig. 8. The average giant component G_N vs tolerance parameter α

Here we consider the cascading failures triggered by removing a single edge. To measure the network functionality we consider the size of the giant component G. We illustrate how this model works in practice by considering random network and scale-free network. Random network can be generated by the Erdős-Rényi model [11], where each pair of nodes is linked with probability p. To generate scale-free network we use standard Barabàsi-Albert model [12]. In both cases we have constructed networks with N=1000 nodes. For random network, edge probalility has been set to $p = 0.005$. In scale-free model, starting from $N_0 = 3$ nodes, one node with $m = 2$ edges is attached iteratively.

To measure the robustness degree of the whole networks against cascading failures, we remove every edge in a network one by one and calculate the corresponding results, e.g., removing edge i and calculating G_i after the cascading process is over. To quantify the robustness of the whole network, we adopt the average giant component, i.e., $G_N = \frac{1}{|E|}\sum_{i\in E} G_i$. The set of edges in the network is denoted with E. The results in function of the tolerance parameter α

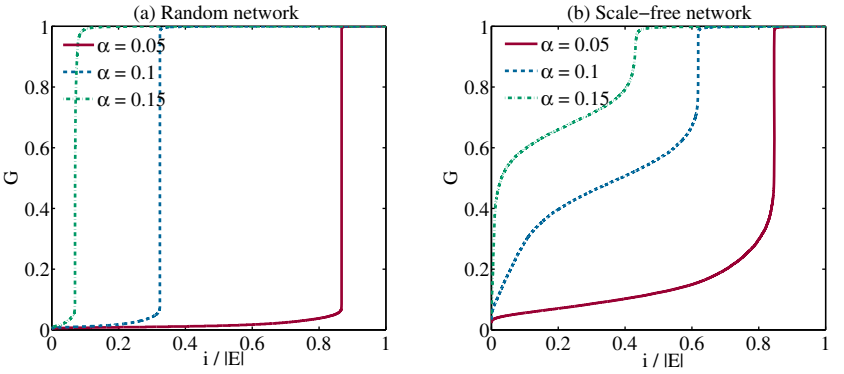

Fig. 9. The giant component size distribution after the system has relaxed to a stationary state for (a) random network and (b) scale-free network

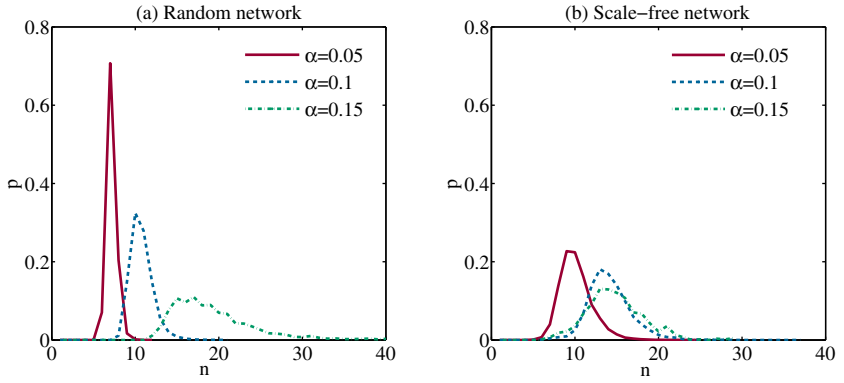

Fig. 10. Probability distributions for the total number of step n of the cascade failure for (a) random network and (b) scale-free network

are summarized in Fig. 8. Clearly, a higher value of α results in a larger giant component after cascade failures finished. One can also observe that for small tolerance, i.e., $\alpha < 0.1$, the random network is more sensitive to cascade failures. This changes for larger tolerances, and scale-free network becomes more sensitive due to more heterogeneous distribution of node degrees and capacities in the scale-free network. Fig. 9 plots size of the giant component from all the possible scenarios of removing a single edge in one network. Simulation results for random network show that giant component discontinuously changes value. We can observe that in random network for $\alpha = 0.05$, removal of a single edge will lead to the collapse of the system under overload failures in more than 80% cases. For $\alpha = 0.1$, percentage of critical edges in network is higher than 30%, and for $\alpha = 0.15$ it is about 10%. For the scale-free network, for the same values of α, we obtain continuous change.

To get another insight into the mechanism of the breakdown, we consider histograms of the total number of step n of the cascade failure in which the size of the giant component is reduced by more than 50%, Fig 10. The average number of cascading failure steps n increases with tolerance parameter α. It is interesting to note that both random and scale-free networks will disintegrate in roughly the same time. The main difference is width of the distribution. In case of random network the distribution is very sharp and more then 70% of networks will disintegrate after 8 steps when $\alpha = 0.05$.

5 Conclusion

In this proceeding we demonstrate how theory of complex systems and the statistical physics of networks may provide us with methods for disaster propagation prediction. These methods allow one to gain a better understanding of the dynamics of disaster spreading and to derive results indicating how to fight them best. We have specifically presented three combinations of networks and specific disaster processes on them. These processes interact with given network structure in different ways yet have a generic thread between them - a variability in outcome due to the local properties of the network structure.

As the main parameters, we have considered the overall density of vegetal phase in fire spreading models and tolerance of the edge to increase of the load. By means of simulations and theoretical model, we have examined probability that fire will propagate through fire protection strip. We have also compared uncertainty in prediction of fire propagation rate due to the local inhomogeneities of the vegetation cover. Important conclusion is that uncertainty in fire propagation rate is especially high for less dense vegetation cover and close to fire percolation point. We have also measured uncertainty in cascade failures of network infrastructure. A model where edges have limited capacity is studied. The behavior of random-network was found to be ambiguous. In comparison to scale-free network, with high and medium values of the tolerance parameter (i.e., $\alpha > 0.1$) most the network is prone to failure of the most edges. On the other hand, failure of one of the critical edges, the network will disintegrate completely.

Acknowledgements. The authors acknowledge support by the Ministry of Science of the Republic of Serbia, under project No. ON171017. Numerical simulations were run on the AEGIS e-Infrastructure, supported in part by FP7 projects EGIInSPIRE, PRACE-1IP, PRACE-2IP, and HP-SEE. The authors also acknowledge support received through SCOPES grant IZ73Z0-128169 of the Swiss National Science Foundation.

References

1. Contreras, M.A., Parsons, R.A., Chung, W.: Forest Ecol. Manage. 264, 134 (2012)
2. Motter, A.E., Lai, Y.-C.: Phys. Rev. E 66, 065102 (2002)

3. Smiljanic, J., Stankovic, I.: Physica A, doi:10.1016/j.physa.2013.01.033
4. Newman, E.J., Forrest, S., Balthrop, J.: Phys. Rev. E 66, 035101 (2002)
5. Kalapala, V., Sanwalani, V., Clauset, A., Moore, C.: Phys. Rev. E 73, 026130 (2006)
6. Buzna, L., Peters, K., Ammoser, H., Kühnert, C., Helbing, D.: Phys. Rev. E 75, 056107 (2007)
7. Morandini, F., Silvani, X., Rossi, L., Santoni, P.-A., Simeoni, A., Balbi, J.-H., Rossi, J.L., Marcelli, T.: Fire Safety J. 41, 229 (2006)
8. Bak, P., Tang, C., Wiesenfeld, K.: Phys. Rev. A 38, 364 (1988)
9. Clar, S., Drossel, B., Schwabl, F.: J. Phys. Condens. Matter 8, 6803 (1996)
10. Zinck, R.D., Grimm, V.: Am. Nat. 174, 170 (2009)
11. Bollobás, B.: Random Graphs. Academic, London (1985)
12. Barabási, A.-L., Albert, R.: Science 286, 509 (1999)
13. Zezelj, M., Stankovic, I., Belic, A.: Phys. Rev. E 85, 021101 (2012)
14. Linn, R.R., Winterkamp, J.L., Weise, D.R., Edminster, C.: Int. J. Wild. Fire 19, 179 (2010)
15. Albert, R., Albert, I., Nakarado, G.L.: Phys. Rev. E 69, 025103 (2004)
16. Crucciti, P., Latora, V., Marchiori, M.: Phys. Rev. E 69, 045104 (2004)
17. Motter, A.E.: Phys. Rev. Lett. 93, 098701 (2004)
18. Schäfer, M., Scholz, J., Greiner, M.: Phys. Rev. Lett. 96, 108701 (2006)
19. Buldyrev, S.V., Parshani, R., Paul, G., Stanley, H.E., Havlin, S.: Nature 464, 08932 (2010)
20. Parshani, R., Buldyrev, S.V., Havlin, S.: PNAS 108, 1007 (2011)
21. Simonsen, I., Buzna, L., Peters, K., Bornholdt, S., Helbing, D.: Phys. Rev. E 100, 218701 (2008)
22. Newman, M.E.J., Ziff, R.M.: Phys. Rev. E 64, 016706 (2001)
23. Stanković, I.E., Kröger, M., Hess, S.: Comp. Physics Comm. 145, 371 (2002)
24. Balaž, A., Prnjat, O., Vudragović, D., Slavnić, V., Liabotis, I., Atanassov, E., Jakimovski, B., Savić, M.: J. Grid. Comput. 9, 135 (2011)
25. Li, J., Zhang, S.-L.: Phys. Rev. E 80, 040104 (2009)
26. Stauffer, D., Aharony, A.: Introduction to Percolation Theory, 2nd revised edn. Taylor and Francis, London (2003)
27. Ziff, R.M., Newman, M.E.J.: Phys. Rev. E 66, 016129 (2002)
28. Margerit, J., Séro-Guillaume, O.: Int. J. Heat Mass Transf. 45, 1723 (2002)
29. Kuittu, M.-P., Haataja, M., Provatas, N., Ala-Nissila, T.: Phys. Rev. E 58, 1514 (1998)
30. Méndez, V., Llebot, J.E.: Phys. Rev. E 56, 6557 (1997)
31. Hovi, J.-P., Aharony, A.: Phys. Rev. E 53, 235 (1996)